ELSEVIER

Journal of Alloys and Compounds 356–357 (2003) 3–8

Journal of ALLOYS AND COMPOUNDS

www.elsevier.com/locate/jallcom

The interaction of hydrogen with internally oxidized Pd alloys as illustrated by Pd–Fe alloys

D. Wang[a], T.B. Flanagan[a], R. Balasubramaniam[b,*]

[a]*University of Vermont, Department of Chemistry and Materials Science Program, Burlington, VT 05405, USA*
[b]*Department of Materials and Metallurgical Engineering, Indian Institute of Technology, Kanpur 208016, India*

Received 2 July 2002; accepted 20 November 2002

Abstract

Hydrogen interactions in internally oxidized Pd alloys have been illustrated using Pd–Fe alloys. Internal oxidation of Pd–Fe alloys results in composites consisting of fine dispersions of nano-sized Fe_2O_3 precipitates in a matrix of pure Pd. Hydrogen solubility measurements can be used as a probe to characterize the reversible and irreversible trapping at the metal–oxide interfacial regions. The effect of hydriding and dehydriding (cycling) on solubilities has been characterized. Hydrogen isotherms can be used to characterize the extent of internal oxidation, and understand the effect of the dispersed internal oxides on hysteresis and H capacity.

Keywords: Hydrogen; Hydriding; Pd alloys; Internal oxidation; Characterization

1. Introduction

Upon high temperature exposure (≥700 °C) of a Pd–M alloy to an oxidizing environment, oxygen dissociates at the surface and O atoms dissolve and diffuse to internally oxidize M, where M is a solute more easily oxidizable than Pd, to produce oxide precipitates in a matrix of pure Pd. This is an example of internal oxidation (IO) [1]. As these precipitates are generally nano-sized, the material produced after IO can be termed as nano-oxide dispersed composites. Hydrogen can be used as a probe to help characterize these composites [2–4]. Hydrogen behavior in internally oxidized systems can be monitored either by electrochemical [2] or gas phase [5] methods. Each of these has its advantages. While the electrochemical technique is sensitive to hydrogen chemical potential changes at very low H contents, the gas phase charging method additionally provides information about the results of hydriding and dehydriding (cycling) of the Pd matrix. Kirchheim and co-workers utilized the electrochemical technique to charge hydrogen and study hydrogen trapping, hydrogen solubilities and diffusion in internally oxidized alloys like Pd–Al, Pd–Mg, Pd–Zr and Pd–Zn [2–4].

2. Interaction of hydrogen with internally oxidized Pd alloys

Two important variables in IO (temperature and time) control the extent of internal oxidation. IO progresses by the movement of the IO front from the surface into the material. This movement is limited by the permeation of oxygen from the surface to the IO zone front. In case the IO front has not fully penetrated the material, partial internal oxidation results, wherein the region from the surface inward is composed of nano-sized oxides in a matrix of pure metal, e.g. Pd, while the inner region will be the unoxidized alloy. The hydrogen solubilities in these regions differ and therefore H solubilities can be used to probe these differences. Noh et al. [5] have shown that after complete IO of Pd–Al alloys, the hydrogen isotherm corresponds to one of pure Pd, while after partial IO, the H_2 isotherm consists of two parts: one corresponding to pure Pd–H and the other to the unoxidized Pd–Al alloy. Therefore hydrogen isotherms can be used to determine the fraction of IO. Hydrogen isotherms following the IO of ternary Pd alloys revealed several additional interesting features [6].

The thermodynamic stability of the internal oxide and its interaction with hydrogen is also of interest. The oxide that forms in Pd–Al alloys is alumina [7,8], in Pd–Y alloys it is yttria [9], and a mixed oxide $PdRhO_2$ forms in Pd–Rh

*Corresponding author.
E-mail address: bala@iitk.ac.in (R. Balasubramaniam).

0925-8388/03/$ – see front matter
doi:10.1016/S0925-8388(03)00164-6

alloys [10,11]. A thermodynamically more stable oxide results in smaller precipitate sizes [1]. SANS (small angle neutron scattering) measurements revealed a smaller mean particle size in internally oxidized Pd–Al alloys [12] when compared to Pd–Rh alloys [11]. Moreover, a very stable oxide like Al_2O_3 will not be reduced by the dissolved hydrogen whereas a less stable oxide, such as $PdRhO_2$, will be reduced with H_2 (573–623 K) forming PdRh precipitates within the Pd matrix [10,11]. Therefore, hydrogen reduction of internal oxides is a technique for segregating components of a substitutional solid solution binary alloy [10,11].

In internally oxidized Pd–M alloys, a large interfacial area between the internal oxides and Pd matrix is created, i.e. several m^2 per cm^3 composite, which will affect hydrogen solubilities. For example, in the very low hydrogen content region, hydrogen is trapped both irreversibly and reversibly by the interface [2–4]. The irreversibly held hydrogen in Pd–Al alloys was believed to be bonded to unsaturated oxygen atoms at the interface forming an interfacial monolayer, which could be removed by evacuation at elevated temperature, $\geq$573 K [3]. There was a solubility enhancement relative to Pd in the dilute phase region; this H is readily removed by evacuation at 323 K [13]. This was shown to originate from the stress fields of the precipitates [8].

Metallurgical aspects of dislocation formation and stabilization in composite materials can be probed by hydrogen. Hydrogen dissolved in metals segregates to the tensile stress field of dislocations and this segregation leads to readily measurable H_2 solubility enhancements in deformed Pd [12]. H_2 solubility enhancements serve as a convenient way to monitor relative dislocation densities. Larger dislocation densities were observed using dilute phase H_2 solubilities in Pd/Al_2O_3 composites compared to Pd after cycling through the hydride phase and after subsequent annealing [14]. Moreover, significantly higher temperatures are needed to remove the dislocations introduced by cycling a $Pd_{0.97}Al_{0.03}$ alloy after IO at 1073 K than pure Pd. The annealing temperature needed to remove dislocations in the alloy after IO at 1273 K was comparable to Pd. Therefore, H_2 solubility measurements reveal that closely spaced precipitates resulting from IO at 1073 K stabilize the dislocation array produced by cycling, whereas the larger and further spaced precipitates formed after IO at 1273 K do not significantly stabilize the dislocations [13]. This is in agreement with what is known about dispersion hardening by internal oxidation [1].

3. Pd/Fe_2O_3 composites

In the present communication, the interaction of hydrogen in the internally oxidized Pd alloys would be illustrated with Pd–Fe alloys. Internal oxidation of Pd–Fe alloys has been recently utilized to determine the diffusion constant of dissolved oxygen in Pd [15]. The slow step in IO is believed to be the diffusion of dissolved oxygen and therefore the movement of the IO front allows determination of the oxygen diffusion constant. The Pd–Fe alloys met this criterion of a well-defined internal oxidation front with the diffusion constant of Fe quite small in comparison to that of oxygen [15].

4. Experimental

The Pd–Fe alloys were prepared by arc-melting the pure elements under argon. The buttons were flipped and remelted several times. They were then annealed in vacuo for 3 days at 1133 K, rolled into foils and then re-annealed for 2 days at 1133 K. The alloys were then oxidized in air at several different temperatures from 973 to 1273 K for various lengths of time. They were quenched after internal oxidation in order to avoid the oxidation of Pd.

5. Results and discussion

5.1. Material characterization

The microstructure after IO and hydrogen interactions can be characterized by a wide variety of techniques. After internal oxidation at 1073 or 1098 K, weight gain measurements indicate that the internal oxide possesses a stoichiometry close to Fe_2O_3, as reported by Gegner [15] after internal oxidation at 1273 K. In the case of Pd–Fe alloys, therefore, the internal oxide is independent of the internal oxidation temperature.

Scanning electron microscopy (SEM) shows that pure Pd nodules form on the surface after IO, resulting from the compressive stresses that are generated within the Pd matrix during internal oxide formation [16,17]. Upon hydrogen cycling, a considerable number of grain boundaries were cracked in the case of Pd–Al alloys [18], while such cracks were not observed for Pd–Fe alloys. The cracked grain boundaries in internally oxidized Pd–Al alloys exhibit a honeycomb-like appearance and there is an increase in surface area after IO and cycling. This results in enhanced rates of hydrogen absorption [18].

Transmission electron microscopy (TEM) reveals the shape of the internal oxides, their distribution and dislocation densities. $Pd_{0.99}Fe_{0.01}$ alloy samples, internally oxidized at 1063 and 1273 K, were examined in a TEM. Both specimens showed large dislocation densities with the lower oxidation temperature having a greater density. This differs from the TEM of internally oxidized Pd–Al alloys where few dislocations were observed [7,8]. Dislocations are created, after IO, due to relaxation of some of the thermal residual stresses that are generated on cooling the material after internal oxidation. The elastic constants (elastic modulus and Poisson's ratio) for iron oxides are lower than that of alumina [19]. The differences in elastic

properties of the oxides are reflected in the relaxation of part of the thermal stresses in internally oxidized Pd–Fe alloys by dislocation punching, as evidenced by the higher dislocation densities in the internally oxidized Pd–Fe alloys compared to Pd–Al alloys. The magnitude of the thermal stresses is determined by the size, shape and distribution of the internal oxides formed, and the difference in thermal expansion coefficients of the oxides and the Pd matrix [8]. Electron diffraction in the TEM provides the structure of the internal oxide. In Pd–Fe alloys, the crystalline precipitates were identified as Fe_2O_3. Only very few studies have addressed microstructural features of the Pd matrix after cycling, which leads to an increase in the dislocation densities [8].

SANS measurements were performed for the $Pd_{0.981}Fe_{0.019}$ and $Pd_{0.963}Fe_{0.037}$ alloys after internal oxidation at 1093 K. The alloys showed increased scattering after internal oxidation with the $Pd_{0.963}Fe_{0.037}$ alloy having a greater scattering than the $Pd_{0.981}Fe_{0.019}$ alloy, as expected. Scattering data in absolute units was collected over the momentum transfer (q) range of 0.002 to 0.3 $Å^{-1}$. The large Q data was fitted to Porod's asymptotic relation:

$$C_p = \lim_{q\to\infty} q^4 I(q) \quad (1)$$

where C_p is the Porod scattering constant and $I(q)$ is the scattering in absolute units. The total surface area of the Fe_2O_3 precipitates per unit volume of sample, S_v, can be calculated from the Porod constant by:

$$S_v = \frac{C_p}{\pi \Delta\rho^2} \quad (2)$$

where $\Delta\rho$ is the difference in scattering length density between the Fe_2O_3 precipitates and the Pd matrix. The estimated S_v values are 1.66×10^5 cm^{-1} for $Pd_{0.981}Fe_{0.019}$ and 3.69×10^5 cm^{-1} for $Pd_{0.963}Fe_{0.037}$. For all two phase systems having uniform scattering length densities in each phase, the volume fraction, ϕ, can be determined from the scattering invariant:

$$\phi(1-\phi) = \frac{Q_t}{2\pi^2\Delta\rho^2} \quad (3)$$

where the scattering invariant Q_t is determined from the integration of all the scattering by:

$$Q_t = \int_0^\infty q^2 (d\Sigma/d\Omega)\cdot(q)dq \quad (4)$$

Assuming the scattering is from a size distribution of spherical particles, the volume weighted mean particle radius is then $R_v = 3\phi/S_v$. The mean particle radii were similar for the two alloys, with the higher Fe content alloy exhibiting a slightly smaller mean (10.4 nm for $Pd_{0.981}Fe_{0.019}$ and 8.4 nm for $Pd_{0.963}Fe_{0.037}$). The current q-range cannot probe particles larger than 50 nm. SANS measurements for an internally oxidized $Pd_{0.97}Al_{0.03}$ alloy provided similar numbers [13] while in the case of Pd–Rh alloys, the sizes were larger [11]. The estimated volume fractions (2.9% for $Pd_{0.981}Fe_{0.019}$ and 5.2% for $Pd_{0.963}Fe_{0.037}$) agreed well with the fraction expected if all of the Fe had been oxidized. The trapping sites for H at the interface can be calculated from the S_v values. This gives 5.2×10^{14} and 7.4×10^{14} sites/cm^2 for $Pd_{0.981}Fe_{0.019}$ and $Pd_{0.963}Fe_{0.037}$, respectively, which are reasonable.

5.2. Dilute phase H_2 solubilities

Dilute phase H_2 solubilities reveal irreversible as well as reversible trapping tendencies. As an example, the H_2 solubilities in internally oxidized $Pd_{0.963}Fe_{0.037}$ are plotted as $p_{H2}^{1/2}$ against r in Fig. 1. The initial and repeat dilute phase solubilities were determined before formation of the hydride phase. The initial H_2 solubilities after internal oxidation have positive intercepts along the $r = H/M$ axis indicating irreversible trapping of H at/or near the Pd/oxide interface. In internally oxidized Pd–Fe alloys, the intercepts are nearly directly proportional to the Fe content. After evacuation at 323 K for 2 h, the repeat dilute phase solubility passed through the origin but, otherwise, had a similar shape as the initial solubility. The irreversibly trapped H is not removed by this evacuation (323 K) because, otherwise, the solubility relation would not have passed through the origin.

The solubility enhancement observed in the dilute phase in the internally oxidized alloy indicates reversible hydrogen trapping (Fig. 1) and is related either to thermal residual stress or to dislocation densities from IO, but the former is more likely because the dislocation densities in

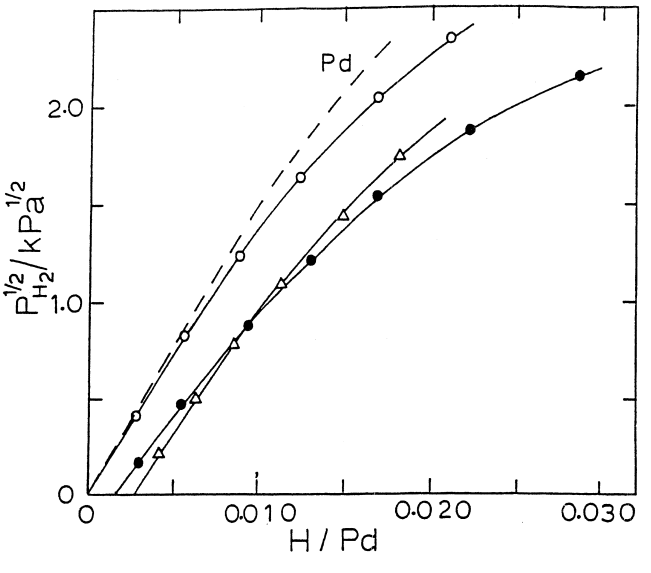

Fig. 1. Dilute phase solubilities (323 K) for the $Pd_{0.963}Fe_{0.037}$ alloy after internal oxidation at 1098 K, 72 h. Dashed line is solubility for pure Pd. The solubility measurements were performed in the following sequence: (△) initial solubility; (○) repeat solubility after evacuation at 323 K for 2 h; (●) solubility after cycling the alloy.

the internally oxidized Pd–Fe alloys before cycling are not that large. For comparable IO conditions, the solubility enhancements are higher for the internally oxidized Pd–Al alloys compared to Pd–Fe alloys. The higher solubility enhancements for the Pd–Al system must be related to the higher residual thermal stresses present in the Pd/Al_2O_3 composites after internal oxidation, which is reasonable because the thermal expansion coefficients of iron oxides are nearly twice that of alumina [19] and hence much closer to that of pure Pd.

The effect of the temperature of IO on H solubilities is interesting (Fig. 2). The $Pd_{0.926}Fe_{0.074}$ alloy internally oxidized at 973 K has a greater dilute phase solubility enhancement relative to Pd than the alloy internally oxidized at 1098 K, which was in turn greater than for the alloy internally oxidized at 1273 K. Lower oxidation temperatures result in smaller precipitates, around which the thermal residual stresses are higher [8]. Moreover, the dislocation densities are also higher after lower oxidation temperatures for internally oxidized Pd–Fe alloys. A consequence of the higher residual stresses and dislocation densities with decreasing temperature is the dilute→hydride transition is very gradual for the alloys internally oxidized at the lower temperatures (Fig. 2).

5.3. Effect of cycling on the intercepts

The internally oxidized alloys were completely hydrided (323 K) and evacuated (cycled). The re-measured dilute phase solubilities are also shown in Fig. 1. The intercepts are finite but smaller than the initial ones. This indicates that some H is removed during cycling and evacuation (323 K) but not all, in contrast to internally oxidized Pd–Al alloys where all of the trapped H is removed (323 K) [13]. There is a nearly linear correlation between the amount of H removed by cycling/evacuation and X_{Fe}. For internally oxidized Pd–Al alloys the removal of the trapped H by cycling/evacuation was suggested to be due to dislocation movement during cycling and interaction with the obstacles, the precipitates; this alters the traps sufficiently to allow removal of the trapped H [13]. This would suggest that in Pd–Fe alloys the more strongly held H is situated within subsurface layers of the Fe_2O_3 precipitates and cannot be removed by dislocation motion.

There is a solubility enhancement after cycling for the internally oxidized alloys with respect to annealed Pd, which increases with X_{Fe}. This solubility enhancement is due to dislocation formation by cycling the internally oxidized alloys. However, relative to the un-cycled, internally oxidized alloys this is small and nearly independent of X_{Fe}.

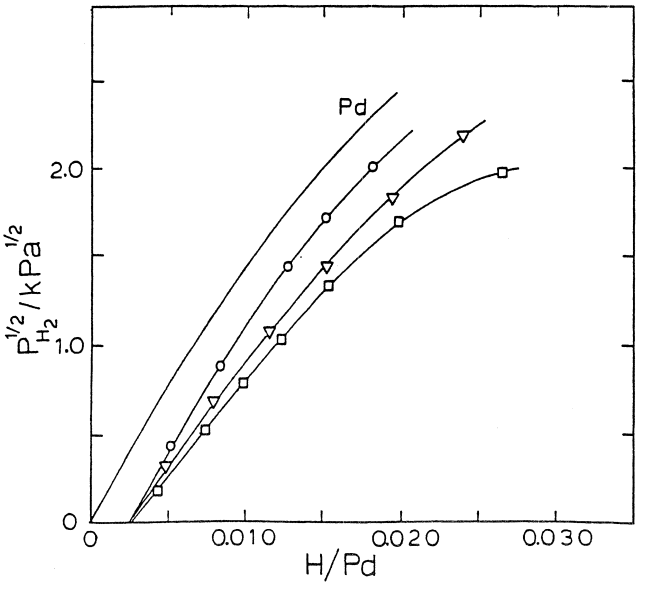

Fig. 2. Dilute phase solubilities (323 K) for the internally oxidized $Pd_{0.926}Fe_{0.074}$ alloy after internal oxidation at (□) 973 K, (▽) 1098 K and (○) 1273 K.

5.4. Complete H_2 isotherms for internally oxidized alloys

The extent of IO can be followed by complete hydrogen isotherms. An isotherm for a partially internally oxidized $Pd_{0.963}Fe_{0.037}$ alloy is shown in Fig. 3 where two plateaux are shown; the lower one corresponds to the internally

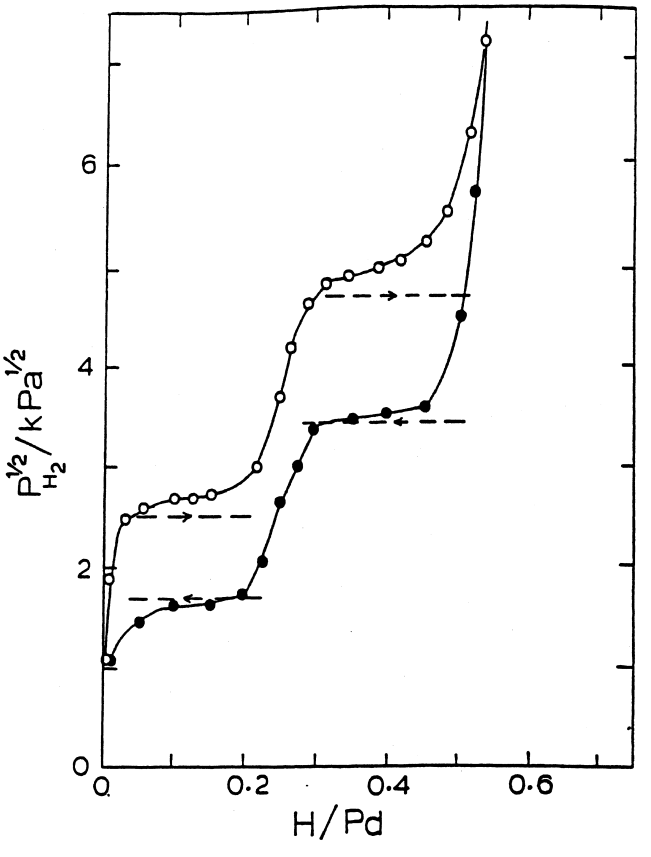

Fig. 3. Isotherms (323 K) for partially internally oxidized $Pd_{0.963}Fe_{0.037}$ alloy (1073 K, 24 h). The open symbols are for absorption and the closed symbols for desorption. The plateau pressures for pure Pd and unoxidized $Pd_{0.963}Fe_{0.037}$ alloy are indicated by the dashed lines.

oxidized portion (Pd–H) and the other to the unoxidized portion of the $Pd_{0.926}Fe_{0.074}$ alloy.

For completely internally oxidized Pd–M alloys, isotherms reveal the effect of internal oxides on hysteresis and capacity. The capacities are generally not affected [5,9]. Complete H_2 isotherms for the internally oxidized (1098 K) $Pd_{0.926}Fe_{0.074}$ alloy are shown in Fig. 4. The initial absorption isotherm is similar to that for the second cycle of Pd but the second and third plateau pressures are higher than the first. After the initial cycle where the trapping occurs, the H capacities are the same as for Pd–H. The desorption plateau is lower than that for Pd–H; a lowering of desorption plateau pressure was found for all of the internally oxidized Pd–Fe alloys with its extent nearly directly proportional to X_{Fe}. Since the hydride formation plateaux for cycles after the initial one are higher than for Pd and the decomposition plateau lower, hysteresis is slightly greater for the internally oxidized Pd–Fe alloys. Interesting differences are found after IO for Pd–Rh alloys, where the absorption plateau is greater than for Pd [11]. After IO of Pd–Al alloys, the initial isotherms are the same as Pd, except that differences appear after cycling [13] and at high temperature, isotherms revealed significant differences in the hysteresis behavior [20].

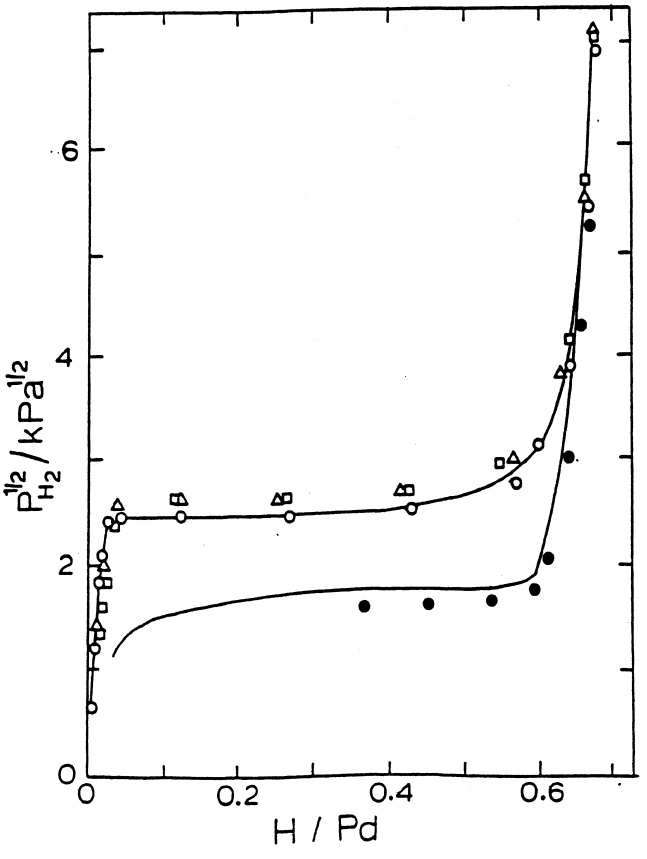

Fig. 4. Isotherms (323 K) for the internally oxidized $Pd_{0.926}Fe_{0.074}$ alloy (1098 K, 72 h): (○) first cycle; (□) second cycle; (△) third cycle; (—) pure Pd second cycle. The open symbols are for absorption and the closed symbols for desorption.

6. Conclusions

The interaction of hydrogen with nano-oxide dispersed Pd composites, prepared by internal oxidation of Pd–M alloys, has been reviewed. Internally oxidized Pd–Fe alloys have been used as an example. Hydrogen can be used as probe to characterize the reversible and irreversible trapping at the metal–oxide interfacial regions by hydrogen solubility measurements. The effect of hydrogen cycling on solubilities has been discussed. Hydrogen isotherms can be used to determine the extent of internal oxidation. They can also be used to help in the understanding of the effect of the internal oxides on hysteresis and hydrogen capacity.

Acknowledgements

T.B.F. wishes to acknowledge financial support from the NSF and R.B. the DST, India and to the University of Vermont for its hospitality while this research was carried out. We acknowledge support of the National Institute of Science and Technology, US Department of Commerce for providing the neutron facilities. Dr. John Barker is thanked for carrying out the SANS studies.

References

[1] J. Meijering, in: H. Herman (Ed.), Advances in Materials Research, Vol. 5, Wiley, New York, 1971, p. 1.
[2] X. Huang, W. Mader, J. Eastman, R. Kirchheim, Scripta Metall. 22 (1988) 1109.
[3] X. Huang, W. Mader, R. Kirchheim, Acta Metall. Mater. 39 (1991) 893.
[4] R. Kirchheim, X. Huang, T. Mütschele, in: N. Moody, A. Thompson (Eds.), Hydrogen Effects on Material Behavior, The Minerals, Metals and Materials Society, 1990, p. 85.
[5] H. Noh, T. Flanagan, R. Balasubramaniam, J. Eastman, Scripta Mater. 34 (1996) 863.
[6] D. Wang, T.B. Flanagan, R. Balasubramaniam, Scripta Mater. 42 (2000) 911.
[7] J. Eastman, M. Rühle, Ceram. Eng. Sci. Proc. 10 (1989) 1515.
[8] R. Balasubramaniam, H. Noh, T. Flanagan, Y. Sakamoto, Acta Mater. 45 (1997) 1725.
[9] W. Zhang, S. Luo, D. Wang, T.B. Flanagan, R. Balasubramaniam, J. Alloys Comp. 330–332 (2002) 607.
[10] D. Wang, T. Flanagan, R. Balasubramaniam, Y. Sakamoto, Scripta Mater. 43 (2000) 685.
[11] D. Wang, J.D. Clewley, T.B. Flanagan, R. Balasubramaniam, K.L. Shanahan, Acta Mater. 50 (2002) 259.
[12] R. Kirchheim, Prog. Mater. Sci. 32 (1988) 261.
[13] D. Wang, H. Noh, S. Luo, T. Flanagan, J. Clewley, R. Balasubramaniam, J. Alloys Comp. 339 (2002) 76.
[14] D. Wang, T.B. Flanagan, R. Balasubramaniam, Scripta Mater. 41 (1999) 517.
[15] J. Gegner, Segregation von Sauerstoff an inner Metall/Oxid-Phasengrenzen, Ph.D. Thesis, Universität Stuttgart, Stuttgart, 1995.
[16] J. Mackert, R. Ringle, C. Fairhurst, J. Dent. Res. 62 (1983) 1229.

[17] R. Balasubramaniam, R. Kirchheim, D. Wang, T.B. Flanagan, J. Alloys Comp. 293–295 (1999) 306.
[18] D. Wang, J.D. Clewley, T.B. Flanagan, R. Balasubramaniam, J. Alloys Comp. 298 (1999) 261.
[19] M. Shütze, in: Protective Oxide Scales and their Breakdown, Wiley, New York, 1997, pp. 17–65.
[20] D. Wang, H. Noh, T.B. Flanagan, R. Balasubramaniam, J. Alloys Comp. 348 (2003) 119.